JOURNAL OF THEORETICAL
AND APPLIED MECHANICS
https://doi.org/10.15632/jtam-pl/202927
ONLINE FIRST

3D STABILITY ANALYSIS OF THE POKER CHIP DETACHMENT PROBLEM

András Levente HORVÁTH*, Attila KOSSA

Department of Applied Mechanics, Faculty of Mechanical Engineering,
Budapest University of Technology and Economics, Műegyetem rkp. 3., H-1111, Budapest, Hungary
*corresponding author, *levente.horvath@mm.bme.hu*

Dry adhesives utilizing the Van der Waals forces are the focus of many applications. Detachment phenomena are especially important to explore in this field. Most previous research was done using axisymmetric models. However, several important cases cannot be analyzed with this simplification. In this work, we build a 3D model to examine the classical "poker chip" problem. We analyze the propagation stability for detachments initiating at the edge of the chip. Novel stability maps are presented for the investigated non-axisymmetric cases. The effect of compressibility and propagation front shape are presented as well.

Keywords: poker chip; adhesion; stability; energy release rate; finite element analysis.

1. Introduction

Throughout history, people have used different types of adhesives. Most commonly, these connect two surfaces by chemical or mechanical bonding mechanisms (Bricotte *et al.*, 2024). In recent decades, another type, called "dry adhesion", has gained the interest of several researchers. This type of adhesion is based on the Van der Waals forces, for which two surfaces need to get in extremely close contact. This type of adhesive has several practical benefits compared to other types. These are well presented by numerous species of animals – mostly reptiles and insects – which utilize this effect (Gorb & Varenberg, 2007; Autumn *et al.*, 2002; Arzt *et al.*, 2003). Among them, the gecko has the largest body mass and remarkable climbing abilities. Geckos are able to rapidly climb smooth and rough vertical surfaces, even when the surface is wet. Their feet strongly bond to the surface, but they can also quickly and reversibly detach from the surface. Animals achieve this by having hierarchical spatula-like hair structures on their feet, allowing them to get sufficiently close to the other surface to exploit the Van der Waals forces. These structures are well visualized in (Varenberg *et al.*, 2010) where several images of various animals are presented using a scanning electron microscope.

Artificial structures mimicking gecko-like adhesion are mostly manufactured from polymer-like materials. These structures have simpler geometry compared to the gecko's feet, utilizing patterns made of pillars. The shape of the contact geometry has a notable effect on adhesion strength and has been studied by many researchers. Hensel *et al.* (2018) studied the effect of the

Ministry of Science and Higher Education
Republic of Poland

The publication has been funded by the Polish Ministry of Science and Higher Education under the Excellent Science II programme "Support for scientific conferences".
The content of this article was presented during the 40th Danubia-Adria Symposium on Advances in Experimental Mechanics, Gdańsk, Poland, September 24–27, 2024.

shape of artificial pillars on adhesion in such structures. Almost all previous research assumes axisymmetric geometry. Hao *et al.* (2024) investigated the importance of considering the effect of nonlinear material behavior and compressibility depending on layer thickness with such a model.

To understand these structures, a better description of the underlying mechanical phenomena is needed. In general, adhesion has been studied using numerical and analytical tools. Both approaches often used the toolset of linear fracture mechanics (Schneider & Swain, 2015; Benvidi & Bacca, 2021). The FEM is well suited for calculating the stored strain energy (U) in the system for arbitrary geometry and material parameters.

Gent and Lindley's (1957) work from the last century is often considered to be the first important contribution regarding the "poker chip" problem. Their research was concerned with material failure, showing that under tensile load, rubber specimens fail under surprisingly low loads due to the triaxial stress state. A decade later Lindsey (1967) published analytical approximations to the normal stress distribution. Since then, several other approximate solutions have been developed, but all of them rely on significant assumptions, like the chip being "thin" and the material being perfectly incompressible (Movchan *et al.*, 2021). They are also limited to axisymmetric cases only. Several other researchers used numerical tools to investigate the internal cracks and cavitation in the material.

The poker chip problem is commonly used to investigate adhesive phenomena. In this case, the interfacial debonding is considered. The poker chip arrangement (see Fig. 1) was used in numerous studies focusing on separation as one of the simplest geometries. Despite being seemingly simple, this setup shows strongly nonlinear behavior regarding, e.g., stress distributions and stored elastic energy. Many more complex geometries (e.g., mushroom, funnel-tip) are used in practice. Their behavior is expected to be even more complex. Thus, it is important to understand the simplest available case as well as possible.

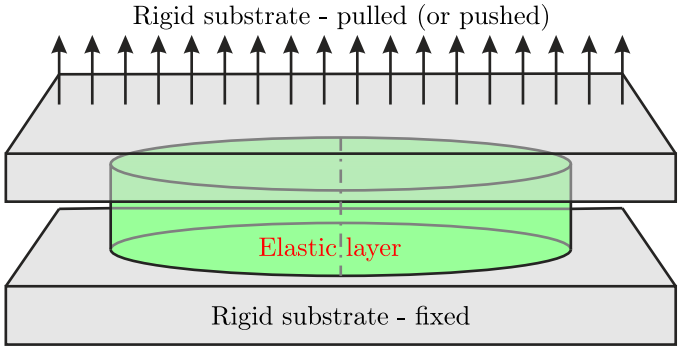

Fig. 1. Poker chip setup.

The most important aspect of previous results for this paper is the importance of the chip thickness and Poisson's ratio regarding detachment stability. The importance and effect of these two parameters are analyzed in detail in (Horváth & Kossa, 2024), where they used an axisymmetric model. They presented stability maps for the axisymmetric edge and center detachment cases. It was shown that the region of stable detachment is narrowed as the thickness of the chip is increased, and there exists a critical thickness above which no stable detachment occurs. Increasing volumetric compressibility slightly decreased the size of the stable zone in these cases.

Local detachment initiated on the outer edge of the poker chip often does not propagate in an axisymmetric way in reality. This can also be observed on the measurements made by Balijepalli *et al.* (2017). In their work, two cases are shown where the detachment initiates from the edge of the chip. In one case the detachment front resembles a circle-like shape, in the other it is closer to straight line. This cannot be investigate with axisymmetric models, which are used in previous studies. The aim of our work is to explore three-dimensional detachment cases initiated on the edge of the poker chip. We created a 3D numerical model to investigate

these previously unexplored cases. We present three stability maps, demonstrating the effect of compressibility as well as shape of the propagating detachment. These basic crack front shapes reveal the previously unknown fundamentals of 3D detachments. Our presented methodology can be extended for more complex, arbitrary detachment propagation fronts.

Section 1 of this article provides an introduction to the topic and summarizes the related literature. Section 2 presents the poker chip problem and the quantities important for our investigation. Section 3 describes the created numerical model and the process used to determine stability. The topic of automated mesh generation is touched upon as well. In Section 4 the obtained novel results are presented, most importantly the stability maps for the investigated cases. Section 5 summarizes the new results. Additionally, the distribution of normal stresses along the contact interface is illustrated in the Appendix at the end of the manuscript.

2. Problem description

The poker chip setup involves a cylindrical elastic solid layer, which is fixed between stiff plates. In real measurements, the elastic layer is made of some polymer, and the plates (substrate) are made of steel. The plates are moved axially, either compressing or pulling the elastic specimen – most research is concerned with the tension case. As the plates are pulled apart, the elastic material may fail due to void nucleation and growing internal cracks. Several papers discussed this in great detail, our work is not concerned with these phenomena (Asp *et al.*, 1995; Kumar & Lopez-Pamies, 2021).

Alternatively, the elastic layer can start to detach from the substrate due to interfacial failure. This scenario is adopted by numerous researchers to study adhesion-related phenomena (Balijepalli *et al.*, 2016). Our work is concerned with this case as well, with detachment propagation stability in the focus. We utilize linear fracture mechanics to study this phenomenon; thus, detachment is modeled as a crack. This approach has been used in multiple previous studies (Antunes *et al.*, 1999; Millwater *et al.*, 2016). The concept of energy release rate is applied. The energy release rate (G) is defined as the decrease of potential energy (π) per unit of contact area (A) decrease:

$$G = \frac{\partial \pi}{\partial A}. \tag{2.1}$$

Note that some papers write G using derivative according to the crack length (which is denoted by a in some papers). This causes the sign of the expression to change. However, in this paper we follow the form adopted by the researchers concerned with detachment and define the energy release rate as per Eq. (2.1).

As a critical value of G is reached (the specific value depends on the strength of the adhesive bond between the surfaces), crack propagation is initiated. Stability analysis is used to determine whether additional external work is needed for the detachment to propagate further. If the detachment process is stable, then additional energy is needed. If the detachment is unstable, the decrease of potential energy will cover the energetic cost of creating the new surface. Thus, the detachment propagates further without the need for additional external work. Stability is determined by the partial derivative of the energy release rate. Importantly, detachment stability does not depend on the type and strength of adhesion between the poker chip and the rigid plate. We investigate a displacement-driven case, thus the potential energy (π) will be equal to the stored strain energy in the system (U). For this reason, investigating the strain energy is sufficient for all of our calculations. Thus, the condition for stable detachment propagation in the displacement-driven case is

$$0 < \frac{\partial G}{\partial A} = \frac{\partial^2 \pi}{\partial A^2} = \frac{\partial^2 U}{\partial A^2}. \tag{2.2}$$

Most previous research focuses on axisymmetric detachments, as this considerably simplifies numerical as well as analytical calculations. In this paper, however, we will not use this assumption, and we will investigate two more general detachment cases. In both cases, detachment is initiated at a single point on the outer edge of the poker chip. In the first case, the detachment propagation front is a straight line. In the second case, the detachment front is circular.

We investigate this problem with numerical tools – FEM specifically. This allows us to investigate quantities that are difficult (or impossible) to measure during experiments. The stored strain energy (U) is easily obtained with FE calculations, making stability evaluation possible.

Our approach matches the method widely adopted by the researchers of adhesion. This makes our results easier to compare to other studies. Detachment is modeled as a crack, but more complex methods, like XFEM or the cohesive zone mode, are not needed for our investigation.

3. Numerical model

Previous research shows that the governing parameters for stability are the relative chip thickness and Poisson's ratio. The polymers used to create artificial structures with dry adhesive properties are usually nearly incompressible. For this reason, many researchers used incompressible models ($\nu = 0.5$). In this paper, the effect of slight compressibility is analyzed as well. The radius of the poker chip is denoted by a. The thickness of the chip is given relative to the radius and it is denoted by h/a. The detachment is characterized by its length along the axis of symmetry in both cases; this length is also compared to the radius and denoted by c/a. The radius is chosen to be $a = 1\,\text{mm}$ during our calculations. The parameters of the model are visualized in Fig. 2. "A" denotes the detachment initiation point, "B" is the last point to detach, and "C" marks the current intersection of the detachment front with the axis of symmetry.

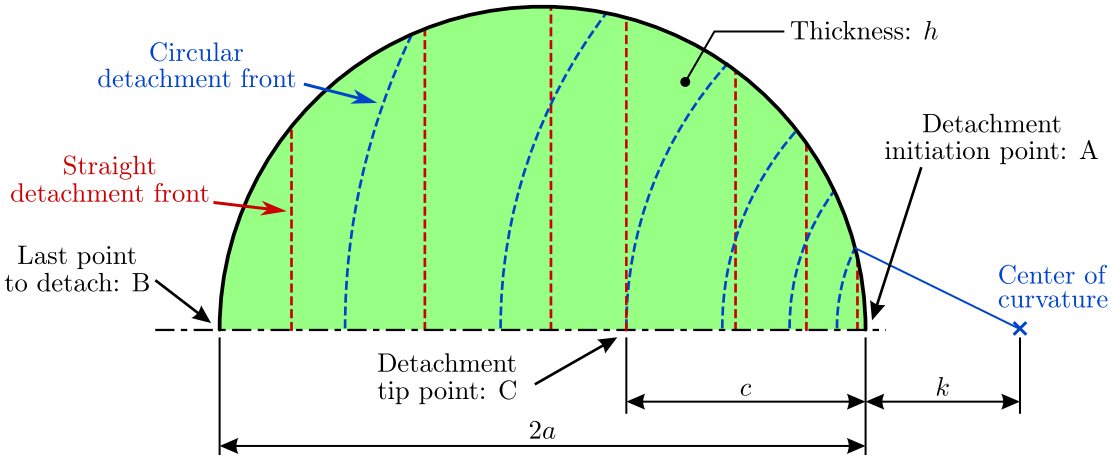

Fig. 2. Model parameters.

As mentioned previously, we consider a case with a straight detachment front and a case with a circular detachment front. Detachment is initiated from the outer edge of the chip. We can describe a circular front with an arbitrary radius using parameter k/a, denoting the dimensionless distance between the detachment initiation point and the center of the circular detachment front. According to the geometry, $0 \leq k/a \leq \infty$. The straight front corresponds to the $k/a = \infty$ limit case. The other investigated case will be the $k/a = 0$ limit, where the initiation point coincides with the center of the circular front.

The chip is modeled with an isotropic linear elastic material, as material nonlinearities can be neglected due the presence of only small strains and deformations in the system. Note that Young's modulus acts as a constant multiplier on U. As derivatives are taken according to Eq. (2.2), it has no influence on the stability properties. During our simulations, we chose $E = 1\,\mathrm{MPa}$.

The non-detached part of the interface is assumed to be perfectly bonded to the rigid substrate – this assumption is also commonly used in the literature to model dry (or other types of) adhesive contact. The substrate material is assumed to be rigid, as commonly used in the literature. The no-slip boundary condition is applied to the non-detached part of the elastic material, which represents perfect bonding to the substrate. The detached part is free to deform, thus no boundary condition is applied there. As the contact with the substrate is well-modeled by the boundary condition and the substrate is assumed to be rigid, it can be fully omitted from the FE model. The meshed model is illustrated in Fig. 4.

The upper interface is prescribed to move by $\overline{u}$ vertically (see Fig. 1). The particular value has no effect on stability, and it is chosen to be $\overline{u} = h/100$ in all simulations.

We built our 3D finite element model in ABAQUS (Dassault Systèmes, 2022). Multiple element types are available for modeling structural 3D problems. After evaluating the options, we predominantly used hex-shaped C3D8(H) elements, but in some cases a few wedge-shaped C3D6(H) elements were also needed to create a well structured mesh. These are general purpose, deformation based linear elements with 8 or 6 nodes respectively. As per ABAQUS recommendations, hybrid formulation was used if Poisson's ratio was greater or equal to 0.495. The problem has planar symmetry, thus a half-model is used to reduce computational costs.

In ABAQUS, our calculation is realized in two simulation steps. The initial step defines the symmetry boundary condition (corresponding to the half model) as well as the no-slip (fixed 0 displacement and rotation) boundary condition on the non-detached part of the interface. These boundary conditions are propagated to the second step, where the prescribed $\overline{u}$ displacement is applied to the top interface.

3.1. Stability calculation

Stability is determined according to Eq. (2.2). The value of U is obtained at several values of detachment length (c/a). Assuming $a = 1$, the contact area (A) is calculated from the detachment length as

$$A = \begin{cases} \frac{1}{4}\left(-\sin\left(2\operatorname{acos}\left(1-c\right)\right) + 2\operatorname{acos}\left(1-c\right)\right) & \text{if } c \leq 1, \\ \frac{1}{4}\left(\sin\left(2\operatorname{acos}\left(c-1\right)\right) - 2\operatorname{acos}\left(c-1\right)\right) + \pi & \text{if } c > 1, \end{cases} \tag{3.1}$$

for the straight detachment front and as

$$A = \frac{\pi c^2}{3} - 0.5\sqrt{c^2 \cdot (2-c)(c+2)} + \operatorname{acos}\left(1 - \frac{c^2}{2}\right), \tag{3.2}$$

for the circular detachment front (assuming $k/a = 0$).

From these relations, the value of $U(A)$ is determined at a series of points. This needs to be differentiated twice to investigate stability. Although several approaches are available to do this, we chose to fit a spline of sufficiently high order on the points of $U(A)$, then carried out the differentiation step on the spline. The exact method for interpolation does not have a notable effect on the obtained values.

These numerical differentiation steps generate small numerical "noise" by nature. This causes the investigated function to oscillate. To mitigate this issue, we applied a Savitzky–Golay filter

to the 2nd derivative. After the filtering, the dataset becomes sufficiently smooth for stability evaluation.

The process of stability evaluation is illustrated in Fig. 3 for one particular case (straight detachment front, $h/a = 0.1$, $\nu = 0.5$). $\overline{U}$ and $\overline{G}$ denote the normalized stored strain energy and energy release rate, calculated as

$$\overline{U} = \frac{U}{U_{\max}} \quad \text{and} \quad \overline{G} = \frac{G}{G_{\max}}. \tag{3.3}$$

Stable regions are denoted by a green background, and unstable regions are shown in red.

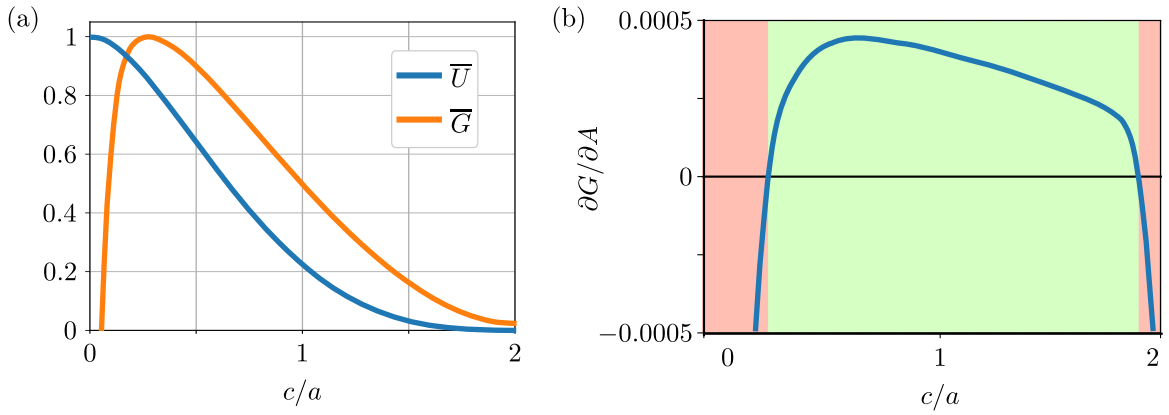

Fig. 3. Illustration of the stability evaluation process (straight detachment front, $h/a = 0.1$, $\nu = 0.5$): (a) normalized strain energy and energy release rate; (b) stability map, green is stable, red is unstable.

3.2. About mesh generation

For creating stability maps with sufficient resolution, several thousands of simulations were needed. For this reason, it was necessary to fully automate mesh generation. The parameters, which influence mesh generation are summarized in Table 1.

Table 1. Parameters describing individual simulations.

Parameter	Possible value
Detachment front shape	Straight or circular
Chip thickness (h/a)	0.01 ... 1.5
Poisson's ratio (ν)	0.5 or 0.48
Detachment length (c/a)	0 ... 1.99

In ABAQUS, the user can control the generated mesh by "seeding" the edges. The following principles were used during the development of the meshing strategy:

- a mesh was characterized by two numbers, one related to the minimum and one to the maximum edge length near the detachment front. These numbers are kept constant for each combination of front shape and h/a;
- the region near the detachment front needs to be the most refined, a smooth transition is needed from the mesh far away from the detachment front;
- the mesh should be well-structured near the detachment front. This means nearly brick-shaped elements with edges parallel/orthogonal to the crack front.

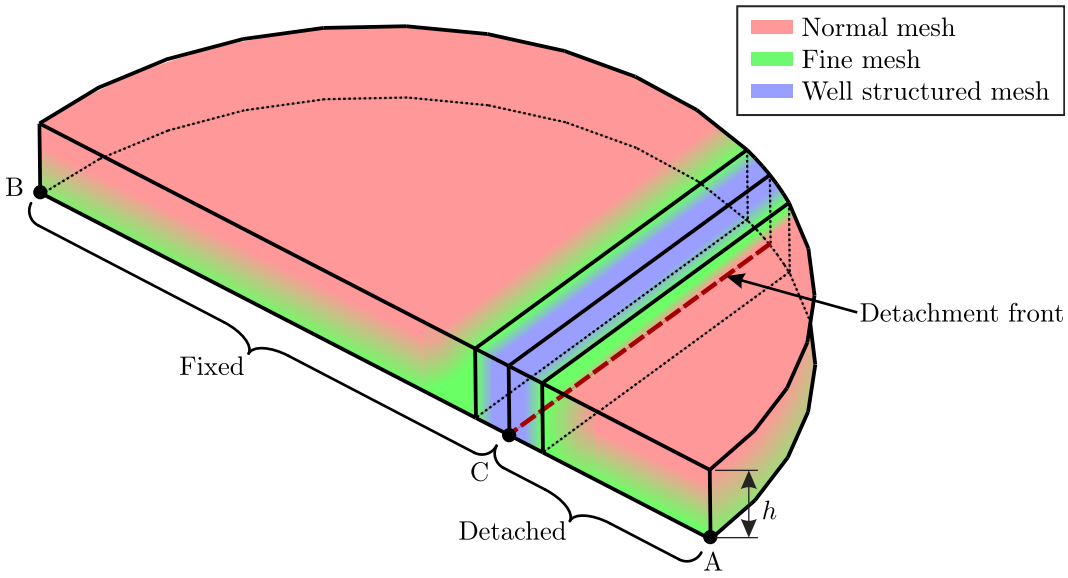

Fig. 4. Illustration of FE model and meshing strategy.

The structure of the mesh is illustrated in Fig. 4. The mesh is well structured in the vicinity of the propagation front, where smaller elements are needed to capture the nonlinear stress distributions.

It is not trivial to fulfill these requirements for the entire range of parameters. In both straight and circular front cases, the main source of problems is the intersection of the detachment front and outer edge of the elastic material. These lines intersect at very shallow angles if c/a is either too small or too large. This leads to highly distorted elements being generated or even failure to generate any mesh – both lead to errors during simulation.

While, in some cases, sharp angles cannot be avoided in the immediate vicinity of the intersection point, these alone did not lead to major issues. Some methods were applied to eliminate mesh generation issues. The meshing strategy was changed based on the value of c/a. If the detachment was very short, the entire detached area was meshed with a uniform dense mesh. As c/a got larger, the entire detached area was meshed as a transition zone. As c/a got sufficiently large, the meshing structure shown in Fig. 4 was used. As cases with almost full detachment were investigated, a similar strategy was applied to those at low values of c/a. First, the left transition zone is extended to the entire non-detached area; then, as full detachment is almost reached, the entire non-detached area is meshed with a uniform dense mesh.

The meshing parameters are chosen so a limit node number is not exceeded by any mesh for a given detachment front shape and h/a. This ensures that computational costs are kept reasonable. Some examples are shown in Table 2.

Table 2. Example node and element numbers for some cases.

Front type	h/a	c/a	Number of nodes	Number of elements
Circular ($k/a = 0$)	0.2	1.6	186802	176505
Circular ($k/a = 0$)	0.2	1.9	188716	178206
Circular ($k/a = 0$)	1.0	0.4	100672	95675
Straight ($k/a = \infty$)	0.4	1.75	99840	93467
Straight ($k/a = \infty$)	0.4	0.15	76470	70876
Straight ($k/a = \infty$)	0.7	0.3	90720	85120

4. Results

Three main cases were investigated. These are a straight detachment front with incompressible material ($\nu = 0.5$) and slightly compressible material ($\nu = 0.48$), then a circular detachment front with incompressible material. The effect of compressibility and shape of the detachment front will be investigated by comparing their respective simulations to the case with the straight detachment front and incompressible material.

The stability map obtained for the straight detachment front and incompressible material case is presented in Fig. 5. Each line for any chip thickness (h/a) is made from 200 simulations; this resolution is sufficiently dense to be drawn as a continuous line. Blue dashed lines denote the interpolated boundary of the stable domain.

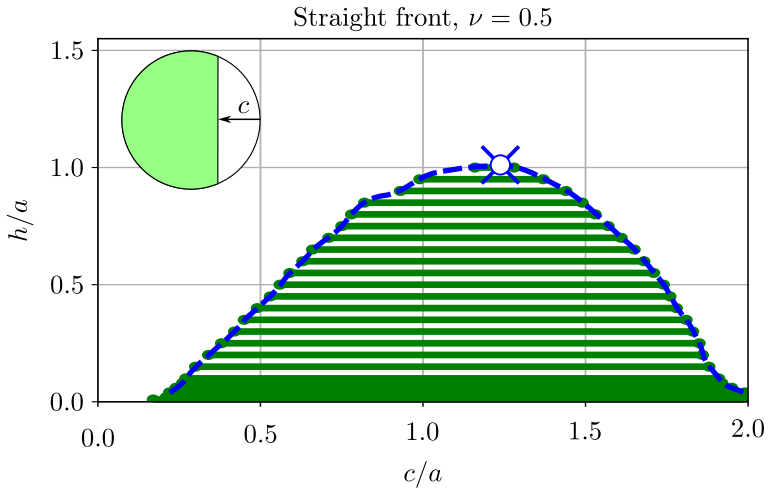

Fig. 5. Stability map for the straight detachment front and incompressible material.

We can see that for any thickness value, detachment propagates in an unstable way after initiation. This unstable region may be followed by a stable segment, and then the final part of the detachment process is unstable once again. For thin chips, the stable region covers almost the whole detachment process. As the chip gets thicker, the stable region starts later and ends sooner. After a critical value of thickness (visible as a blue "X" with a white middle point on the boundary), no stable region exists. This thickness value is denoted by h_{cr}/a, and the corresponding value of detachment length is denoted as c_{cr}/a. Based on the interpolated boundaries, we can calculate the critical values. In the current case $h_{cr} = 1.006$ and $c_{cr}/a = 1.233$. Overall, the limit points of stability follow relatively simple, monotonous trends.

The stability map for the slightly compressible case ($\nu = 0.48$) is presented in Fig. 6. Compared to the previous case, the most noticeable difference is for low thickness values ($h/a \leq 0.3$). A "dent" forms in the stable region and the trend of stability limit points is no longer monotonous. For very thin chips, stability is hard to evaluate, leading to discontinuity in the stable region. The rest of the stable region is qualitatively similar to the incompressible case but quantitatively gets smaller in every direction. This includes a decrease in critical thickness, for this case $h_{cr}/a = 0.957$ and $c_{cr}/a = 1.233$.

The stability map for the circular detachment front case is presented in Fig. 7. The general trends are the same as with the straight detachment front. The stable region is generally quantitatively smaller, but the difference is marginal. The critical thickness changes to $h_{cr}/a = 0.963$ and $c_{cr} = 1.193$. At extremely small thickness values, the stable region is wider. Overall, the change in the propagation front shape results in a surprisingly small difference regarding the stability maps.

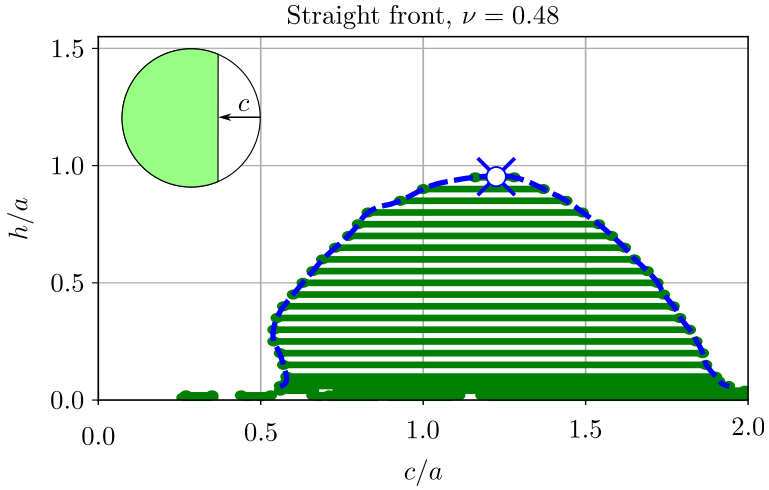

Fig. 6. Stability map for the straight detachment front and slightly compressible material.

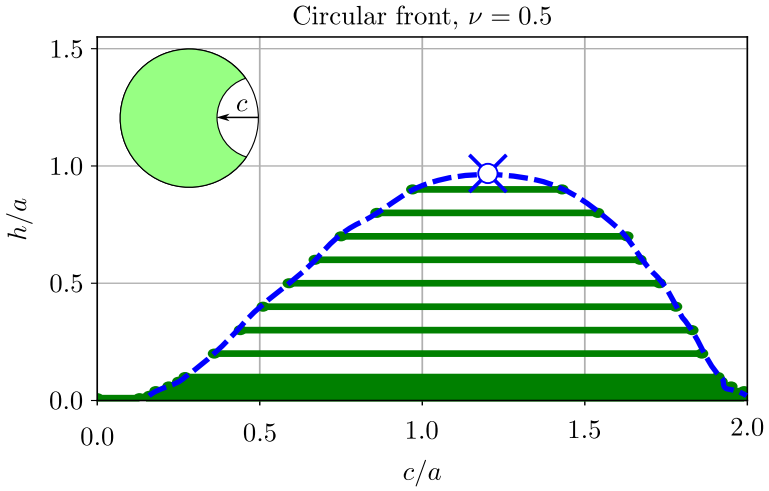

Fig. 7. Stability map for the circular detachment front and incompressible material.

4.1. Stress distributions

The stress distribution is easily obtained from the built model. The mesh is most refined near the detachment front, making the areas with the highest stress gradients the most resolved. The main focus of this paper is detachment stability, not stress distributions. However, we show some of the stress results as well to demonstrate the nonlinearities in the normal stress distributions.

Stresses are normalized by $\overline{\sigma}$, which is the average stress along the contact area. Due to the prescribed vertical displacement $\overline{u}$ on the upper rigid plate, the strain energy U stored in the elastic body is induced. In the absence of energy dissipation, this energy equals the work done by the external force system. With this, the reaction force F generated during loading can be calculated from the strain energy, from which the average normal stress along the contact surface can be calculated as

$$U = \frac{1}{2} F \overline{u} \quad \rightarrow \quad F = \frac{2U}{\overline{\sigma}} \quad \rightarrow \quad \overline{\sigma} = \frac{F}{A}, \tag{4.1}$$

where A is calculated as per Eqs. (3.1) or (3.2).

One illustration of the stress distributions is shown in Fig. 8. We can see that the shape of the crack front has no significant impact on the normal stresses along the symmetry line. The normal stress distributions along the entire contact interface are included in the Appendix.

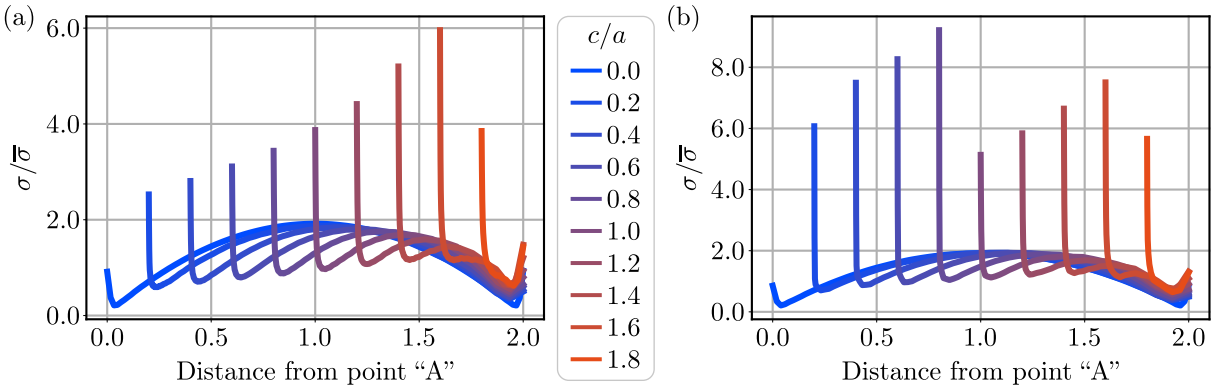

Fig. 8. Illustration of normalized normal stress distributions along the C-B line of symmetry (see Fig. 2), contact interface ($h/a = 0.2$ and $\nu = 0.5$): (a) straight detachment front; (b) circular detachment front.

5. Discussion

The detachment stability of the poker chip problem was investigated in detail using a fully 3D FE model built in ABAQUS. This allowed us to study detachment phenomena, which had previously not been investigated in the literature. In all of the cases considered, the detachment initiated from a point on the edge of the chip. In one case, the detachment front propagated as a straight line. The effect of slight compressibility was also demonstrated using this scenario. In the second case, a circular propagation front was considered.

We analyzed two different crack front shapes: straight and circular. The difference in crack front shape had only a minor effect on the stability maps – the stable region got slightly smaller for the circular front case. These can be considered as two extreme cases: the circular front's center of curvature matches the detachment initiation point. The straight front can be viewed as a circle with an infinite radius, and the center of curvature is infinitely far from the detachment initiation point. Thus, we hypothesize that a circular crack front with an arbitrary center of curvature will produce similar results and have only a minor quantitative effect on the stability of the detachment.

In all the investigated cases, the detachment was initially unstable. This unstable region may be followed by a stable region. The detachment turned unstable once again, nearing complete detachment. The width of the stable region is determined by the chip thickness (h/a). Generally, the thicker the chip gets, the narrower the stable region becomes. For very thin chips, almost the entire detachment process is stable. Above a critical thickness value (h_{cr}/a), no stable region can exist, and the detachment is fully unstable.

The effect of slight compressibility is presented. At low ($h/a \leq 0.3$) thickness values, a noticeable "dent" forms on the stability map – detachment gets stable later. This effect may be relevant for practical applications, as materials that are used to manufacture structures with dry adhesive properties show little, but not negligible, volumetric compressibility. If $h/a > 0.3$, the stable zone shrinks by a small amount.

Appendix – Example: normal stress distribution

The distribution of normal stress on the bottom interface is shown in Fig. 9. In this case $h/a = 0.2$ and $\nu = 0.5$ (these contour plots are not normalized with average stress $\overline{\sigma}$).

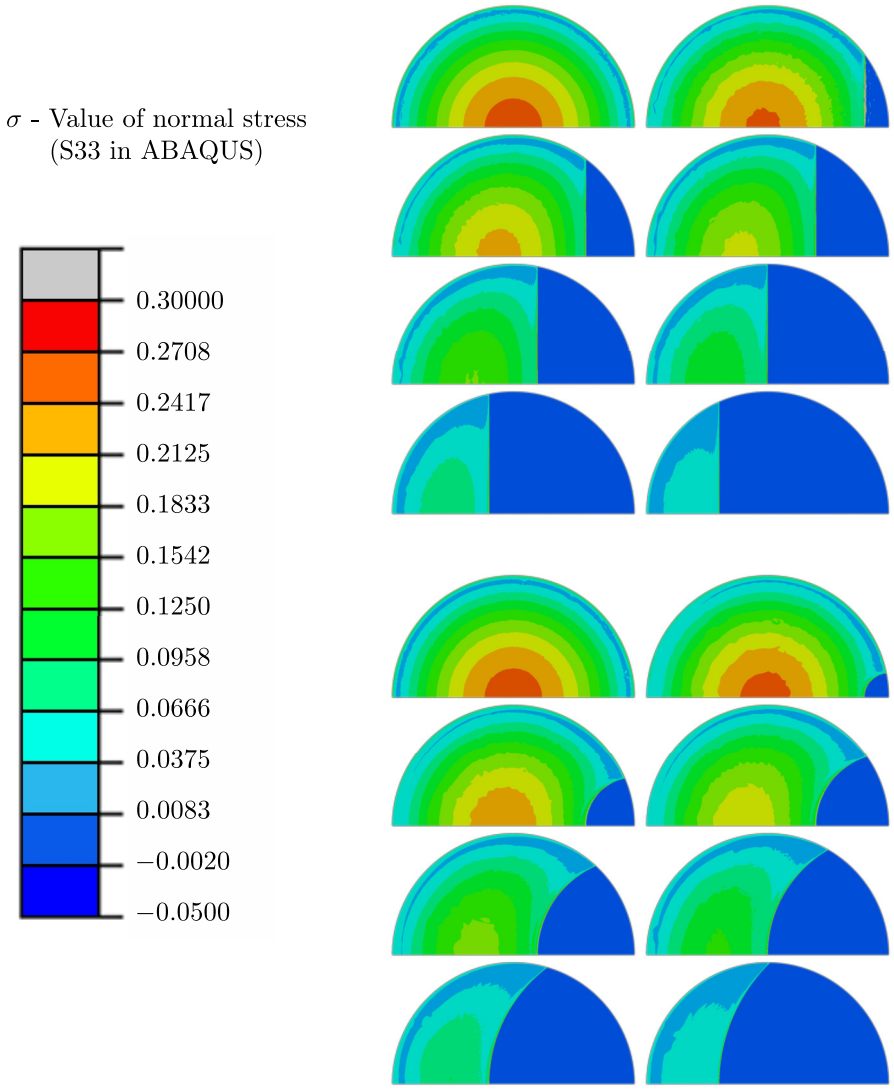

Fig. 9. Normal stress distribution for straight and circular detachment fronts, $h/a = 0.2$, $\nu = 0.5$.

Acknowledgments

This research was supported by the Hungarian National Research, Development and Innovation Office (FK 142457). This research was supported by the János Bolyai Research Scholarship of the Hungarian Academy of Sciences.

References

1. Antunes, F.V., Ferreira, J.M., & Byrne, J. (1999). Stress intensity factor calculation based on the work of external forces. *International Journal of Fracture*, *98*(1), 1–14. https://doi.org/10.1023/A:1018684932071

2. Arzt, E., Gorb, S., & Spolenak, R. (2003). From micro to nano contacts in biological attachment devices. *Proceedings of the National Academy of Sciences*, *100*(19), 10603–10606. https://doi.org/10.1073/pnas.1534701100

3. Asp, L.E., Berglund, L.A., & Gudmundson, P. (1995). Effects of a composite-like stress state on the fracture of epoxies. *Composites Science and Technology*, *53*(1), 27–37. https://doi.org/10.1016/0266-3538(94)00075-1

4. Autumn, K., Sitti, M., Liang, Y.A., Peattie, A.M., Hansen, W.R., Sponberg, S., Kenny, T.W., Fearing, R., Israelachvili, J.N., & Full, R.J. (2002). Evidence for van der Waals adhesion in gecko setae. *Proceedings of the National Academy of Sciences*, *99*(19), 12252–12256. https://doi.org/10.1073/pnas.192252799

5. Balijepalli, R.G., Begley, M.R., Fleck, N.A., McMeeking, R.M., & Arzt, E. (2016). Numerical simulation of the edge stress singularity and the adhesion strength for compliant mushroom fibrils adhered to rigid substrates. *International Journal of Solids and Structures*, *85–86*, 160–171. https://doi.org/10.1016/j.ijsolstr.2016.02.018

6. Balijepalli, R.G., Fischer, S.C.L., Hensel, R., McMeeking, R.M., & Arzt, E. (2017). Numerical study of adhesion enhancement by composite fibrils with soft tip layers. *Journal of the Mechanics and Physics of Solids*, *99*, 357–378. https://doi.org/10.1016/j.jmps.2016.11.017

7. Benvidi, F.H., & Bacca, M. (2021). Theoretical limits in detachment strength for axisymmetric bimaterial adhesives. *Journal of Applied Mechanics*, *88*(12), Article 121007. https://doi.org/10.1115/1.4052107

8. Bricotte, L., Chougrani, K., Alard, V., Ladmiral, V., & Caillol, S. (2024). Adhesion theories: A didactic review about a century of progress. *International Journal of Adhesion and Adhesives*, *132*, Article 103673. https://doi.org/10.1016/j.ijadhadh.2024.103673

9. Dassault Systèmes (2022). Abaqus version 2022.

10. Gent, A.N., & Lindley, P.B. (1957). Internal flaws in bonded cylinders of soft vulcanized rubber subjected to tensile loads. *Nature*, *180*, 912–913. https://doi.org/10.1038/180912a0

11. Gorb, S.N., & Varenberg, M. (2007). Mushroom-shaped geometry of contact elements in biological adhesive systems. *Journal of Adhesion Science and Technology*, *21*(12–13), 1175–1183. https://doi.org/10.1163/156856107782328317

12. Hao, S., Huang, R., & Rodin, G.J. (2024). Constitutive models for confined elastomeric layers: Effects of nonlinearity and compressibility. *Mechanics of Materials*, *190*, Article 104912. https://doi.org/10.1016/j.mechmat.2024.104912

13. Hensel, R., Moh, K., & Arzt, E. (2018). Engineering micropatterned dry adhesives: From contact theory to handling applications. *Advanced Functional Materials*, *28*(28), Article 1800865. https://doi.org/10.1002/adfm.201800865

14. Horváth, A.L., & Kossa, A. (2024). Stability maps for the slightly compressible poker chip detachment problem. *Finite Elements in Analysis and Design*, *242*, Article 104257. https://doi.org/10.1016/j.finel.2024.104257

15. Kumar, A., & Lopez-Pamies, O. (2021). The poker-chip experiments of Gent and Lindley (1959) explained. *Journal of the Mechanics and Physics of Solids*, *150*, Article 104359. https://doi.org/10.1016/j.jmps.2021.104359

16. Lindsey, G.H. (1967). Triaxial fracture studies. *Journal of Applied Physics*, *38*(12), 4843–4852. https://doi.org/10.1063/1.1709232

17. Millwater, H., Wagner, D., Baines, A., & Montoya, A. (2016). A virtual crack extension method to compute energy release rates using a complex variable finite element method. *Engineering Fracture Mechanics*, *162*, 95–111. https://doi.org/10.1016/j.engfracmech.2016.04.002

18. Movchan, A.B., Rebrov, K.R., & Rodin, G.J. (2021). Axisymmetric deformation of compressible, nearly incompressible, and incompressible thin layers between two rigid surfaces. *International Journal of Solids and Structures*, *214–215*, 61–73. https://doi.org/10.1016/j.ijsolstr.2020.12.002

19. Schneider, G.A., & Swain, M.V. (2015). The Schwickerath adhesion test: A fracture mechanics analysis. *Dental Materials*, *31*(8), 986–991. https://doi.org/10.1016/j.dental.2015.05.007

20. Varenberg, M., Pugno, N.M., & Gorb, S.N. (2010). Spatulate structures in biological fibrillar adhesion. *Soft Matter*, *6*, 3269–3272. https://doi.org/10.1039/C003207G

Manuscript received December 15, 2024; accepted for publication March 13, 2025; published online July 2, 2025.